

ANALYSIS OF THE PHYSICAL ORIGIN OF TRAP CENTRES AND THEIR EFFECT ON SOLAR CELLS

^{1a}Paul Gundel, ¹Martin Schubert, ²Matthias Allardt, ¹Wilhelm Warta
¹Fraunhofer-Institute for Solar Energy Systems ISE
Heidenhofstr. 2, 79110 Freiburg, Germany
^{1a}paul.gundel@ise.fraunhofer.de

²Dresden University of Technology
Institut für Angewandte Physik, Professur für Halbleiterphysik, 01062 Dresden, Germany

ABSTRACT: Defect sites in silicon, which temporarily capture excess charge carriers (traps), are a promising source of information on defect structures relevant for PV-application of the material. In this work the correlation between traps in p-type silicon, structural crystal defects and impurities is explored in order to find the origin of these traps in multicrystalline silicon. The trap density is compared to the density of different impurities and structural crystal defects. These comparisons reveal that the trap density is positively correlated to the oxygen density and negatively correlated to the density of the metallic impurities analyzed. In addition we show that structural crystal defects are necessary but not sufficient for the existence of high trap densities. The properties of these structural defects are further investigated by photoluminescence. In summary, structural crystal defects which are decorated by oxygen precipitates arise as likely origin of trap centers.

Keywords: Defects, Diffusion length, Dislocation, Impurities, Trapping

1 INTRODUCTION

An anomalous increase of the apparent excess carrier lifetime due to trapping of minority carriers under low injection conditions has been reported in many publications. This effect is generally assumed to be caused by trapping of minority carriers [1,2], a concept which is supported by both injection and temperature dependent measurements [3,4]. In 1953 Fan [5] and in 1955 Hornbeck and Haynes [6] independently developed a theoretical model to describe this trapping of minority carriers. According to recent publications this effect is correlated to dislocations [1,7,3], but the origin of trap centers in multicrystalline silicon is still unclear, whereas in Czochralski silicon oxygen was related to the trapping effect [8].

In this paper the spatially resolved trap density is determined by injection dependent Carrier Density Imaging / Infrared Lifetime Mapping (CDI/ILM) measurements [7,3]. From these measurements the trap density can be extracted by fitting the Hornbeck-and-Haynes model to the experimental data [9,7,3]. First the spatially resolved trap density is compared to the structural crystal defect density, which shows, that structural crystal defects are necessary but not sufficient in order to create high trap densities. The second goal is to determine the further requirements, which need to be fulfilled for the existence of high trap densities. For this purpose the trap density is compared to different metallic impurity densities and the effect of two different annealing steps on the trap density in Czochralski silicon is examined: First the effect the Cz-specific defect on the trap density is investigated in detail. Secondly the effect of an annealing step at 800 °C is studied. In order to find the impact of oxygen on the trap density in multicrystalline silicon the trap density of an as-cut multicrystalline wafer, which is vertically cut out of an ingot, is measured and compared to the diffusion length of the solar cell that is processed from this wafer. All samples in this paper are p-type boron doped and have no

surface passivation (unless otherwise noted), in order to avoid a possible distortion of the results by a depletion region at the surface due to a non-optimal passivation layer. This may cause Depletion Region Modulation (DRM) under injection, an effect, that can be mistaken for an increased trapping effect. In ref. [7,10] it was shown that a good surface passivation or an unpassivated surface have no major influence on the trap density.

2 EXPERIMENTAL

2.1 Trap density imaging

Free minority carriers can be trapped in shallow trap levels or levels with asymmetric capture cross sections for holes and electrons [6,5]. Charge neutrality requires that the trapped minority carriers are compensated by additional majority carriers in steady state condition. Lifetime measurements such as CDI/ILM are based on the assumption, that the excess majority carrier density equals the excess minority carrier density. This assumption does not hold anymore for low injection if trapping occurs. Since CDI/ILM detects the absorption and emission of both, majority and minority carriers, CDI/ILM measures a higher apparent lifetime than the actual recombination lifetime in low level injection. Trapping leads to an increasing apparent lifetime with decreasing injection density. The injection dependence of the apparent lifetime τ_{app} following the Hornbeck-Haynes model for p-type silicon is [7]:

$$\tau_{app}(\Delta n) = \frac{1}{\alpha_n + \alpha_p} \tau_{rec} \left[\alpha_n + \alpha_p \left(1 + \frac{n_T(\Delta n)}{\Delta n} \right) \right]. \quad (1)$$

With α_n and α_p being the free carrier absorption coefficients for electrons respectively holes, τ_{rec} is the recombination lifetime which is assumed to be injection independent in low injection, Δn the excess minority carrier density and n_T the density of trapped minority

carriers, which depends on the trap density N_T and the trap escape ratio r_{esc} ¹:

$$n_T = \frac{N_T \Delta n}{\Delta n + N_T r_{esc}} \quad (2)$$

By fitting this model to a low injection CDI-measurement at each point of a wafer a trap density image can be deduced [9,7]. A qualitative image of the trap density can be obtained by a single CDI/ILM measurement at very low injection [10].

For the determination of the trap densities in our experiments the generation rate was varied between $1.98 \times 10^{14} \text{ cm}^{-2}\text{s}^{-1}$ and $2.21 \times 10^{17} \text{ cm}^{-2}\text{s}^{-1}$, which leads to an injection level in our samples between approximately $2 \times 10^{10} \text{ cm}^{-3}$ and $5 \times 10^{13} \text{ cm}^{-3}$. Since these injection levels are very small compared to the doping concentrations of $3.5 \times 10^{15} \text{ cm}^{-3}$ to $1.5 \times 10^{16} \text{ cm}^{-3}$, the effective recombination lifetime can be assumed to be injection independent with sufficient accuracy.

2.2 Imaging of structural crystal defects

To measure the spatially resolved structural crystal defect density of a large wafer area (up to $156 \times 156 \text{ mm}^2$) qualitatively, the polished wafer is etched in a Secco etch for about five minutes. The Secco etch preferentially attacks the wafer surface where structural crystal defects are present leading to local etch pits. Since rough surfaces result in a significantly higher emissivity in the infrared range than flat surfaces [11], a qualitative image of the structural crystal defect density can be obtained by taking a picture of the etched wafer with an infrared camera. Areas with high structural crystal defect densities appear bright and areas with low structural crystal defect densities dark, if the wafer temperature is higher than the background temperature.

3 RESULTS

3.1 Correlation of traps with structural crystal defects

The qualitative trap density distributions of two cut-outs from different as-cut wafers are compared with the structural crystal defect densities. The qualitative trap density was quantitatively confirmed by fitting the Hornbeck-and-Haynes model to injection dependent measurements with lower spatial resolution. One of the wafers originates from the top region of a standard multicrystalline ingot, the other one from the bottom region of this ingot. The thickness of both wafers is $(270 \pm 5) \mu\text{m}$, the doping concentration is about $9.9 \times 10^{15} \text{ cm}^{-3}$.

The structural crystal defect density and the trap density show a high positive correlation in the wafer from the bottom of the ingot (figs. 1, 2), which is in good agreement with [1,7,3]. In the wafer of the top region there is a positive correlation in some areas, but there are also regions with high structural crystal defect densities and simultaneously low trap densities (figs. 3, 4). Since the trap density of the wafer from the bottom is about one order of magnitude higher than the trap density of the wafer from the top, fig. 1 and fig. 3 have different color scales. We conclude that structural crystal defects are required for the existence of high trap densities in this sample, but additional conditions such as specific impurity decorations must be fulfilled.

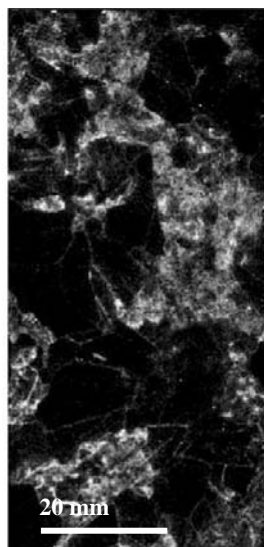


Figure 1: Qualitative trap density of the wafer from the bottom of the ingot. High trap densities are bright.

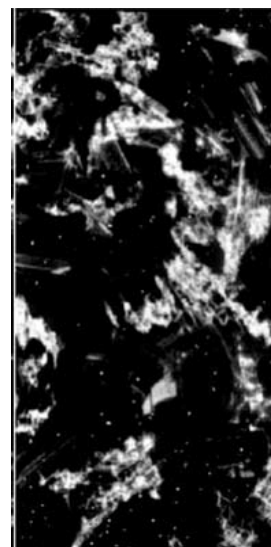


Figure 2: Qualitative structural crystal defect density of the same area that is depicted in Fig. 1. High structural crystal defect densities are bright. The image shows a high positive correlation with the trap density.

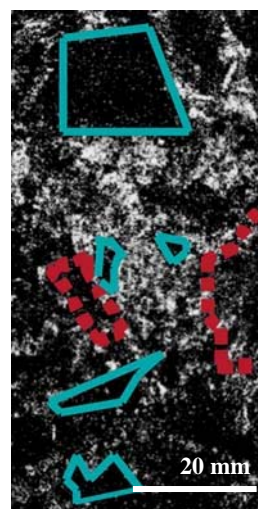


Figure 3: Qualitative trap density of the wafer from the top of the ingot. High trap densities are bright.

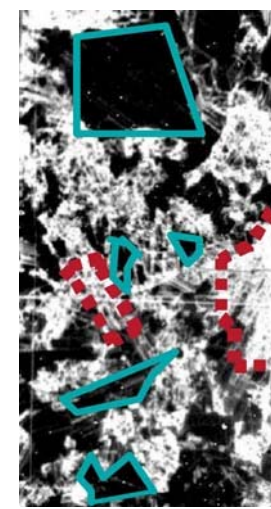


Figure 4: Qualitative structural crystal defect density of the same area that is depicted in Fig. 3. High structural crystal defect densities are bright. In some areas (i.e. the cyan marked areas) there is a positive correlation between trap density and structural crystal defect density, but there are also areas with high structural crystal defects and low trap densities (i.e. red marked areas).

To examine the physical difference between crystal defects with and without increased trap density, the photoluminescence spectra of a location with high crystal defect density and high trap density on the one hand and a location with high crystal defect density and low trap density on the other hand were measured at 4.2 K. The excitation laser was a 514 nm Argon laser. Crystal defects which exhibit an increased trap density also exhibit a different photoluminescence spectrum from those with a low trap density, as depicted in fig. 5.

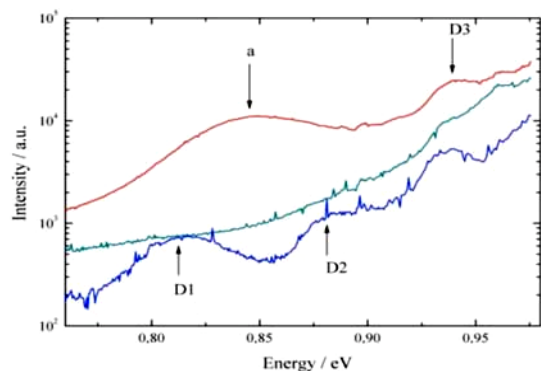


Fig. 5: Photoluminescence spectra of three samples. Two with high crystal defect densities, one of these with high trap density (blue line) and one with low trap density (red line). As reference a spectrum of a sample with low crystal defect density is shown (cyan line).

The sample with the high trap density emitted a spectrum with clearly resolved defect peaks, which can be attributed to the well known D-lines. In detail D1 at 0.81 eV, D2 at 0.88 eV and D3 at 0.93 eV could be observed. In contrast the photoluminescence spectrum of the sample with low trap density was dominated by a broad band centered at 0.84 eV and also the D3-line appeared, but D1 and D2 could not be observed. This is a strong indication that dislocations with a high trap density differ significantly from those with a low trap density in their physical properties.

The suggestion that structural crystal defects do not necessarily lead to high trap densities was confirmed by an injection dependent CDI/ILM measurement of a $3.5 \times 10^{15} \text{ cm}^{-3}$ gallium doped multicrystalline wafer with Float Zone purity, which showed an extremely low trap density of less than $2 \times 10^{11} \text{ cm}^{-3}$. This means that traps mark dislocations, which are decorated by impurities and therefore particularly detrimental to the solar cell performance. In the following impurities are examined, which could cause an increased trap density. The surface of this wafer is polished and unpassivated, the wafer thickness is $(660 \pm 5) \mu\text{m}$. More details on the sample can be found in [12]. In ref. [8] it was shown that boron and gallium doping lead to similar trap densities. In the following the influence of impurities on the trap density is explored.

3.2 Influence of impurities

The trap densities of intentionally contaminated and SiN passivated monocrystalline floatzone wafers, with a thickness of $(390 \pm 15) \mu\text{m}$ and a doping concentration of $1.5 \times 10^{16} \text{ cm}^{-3}$, are determined and compared to the impurity concentrations. The contamination was done in the melt and the impurity concentrations were measured

with Neutron Activation Analysis [13]. The wafers probably have an unusual high crystal defect concentration due to their small diameter, which led to a high cooling rate, more details on the samples can be found in [13]. The high defect concentration can be deduced from the low minority carrier lifetime (smaller than $10 \mu\text{s}$) of a reference sample, that was not contaminated. Parts of the ingots were annealed to ease the sawing of the wafers. The results of the trap density measurements are presented in fig. 6 and fig. 7 against metal impurity concentration. Fig. 6 and fig. 7 demonstrate that iron and molybdenum impurities can reduce the trap density.

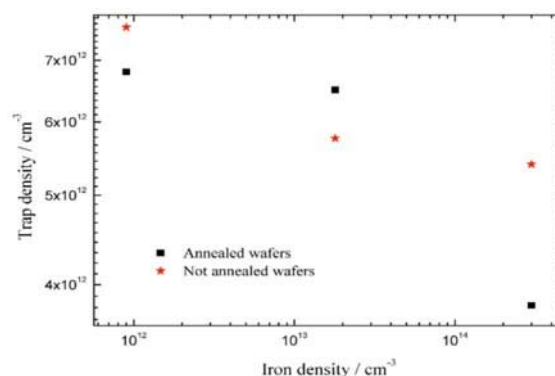


Figure 6: Trap density plotted against iron density. The trap density shows the tendency to be reduced by iron.

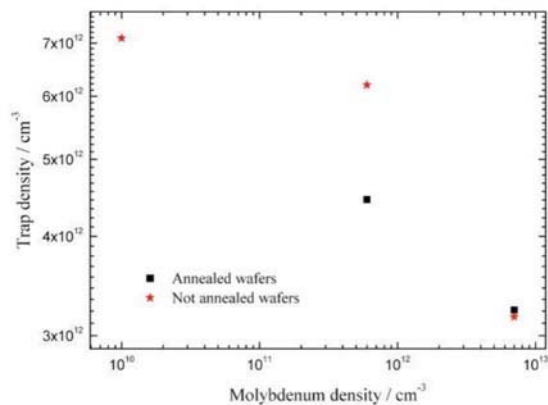


Figure 7: Trap density plotted against molybdenum density. As for iron, molybdenum shows the tendency to reduce the trap density.

A comparable trend was observed in intentionally iron and intentionally titanium contaminated directionally solidified multicrystalline wafers. In [14] the concentration of dissolved iron and chromium in floatzone wafers was shown not to be correlated to the trap density. Thus, the accumulation of metallic impurities at structural crystal defects could explain the existence of areas with high structural crystal defect densities and low trap densities in fig. 3 and fig. 4. The metallic impurities induce deep energy levels within the bandgap. This could cause recombination of the trapped electrons via the deep defect levels. Since a recombination of trapped electrons is neglected in the Hornbeck-Haynes model, this would result in a lower measured trap density.

3.3 Trapping in Czochralski wafers

In boron doped Czochralski wafers a metastable defect was found [15,16], which reduces the minority carrier lifetime in Czochralski wafers, when it is in its activated state. This Cz-specific defect can be activated by illumination and passivated by a heat treatment^{15,16}. The defect is attributed to boron oxygen complexes BO_{2i} [17]. By the heat treatment the complexes are dissolved and oxygen and boron are released. In [8] the effect of the Cz-specific defect on the trap density was examined and the trap density was found to be increased in the activated defect state compared to the passivated state. We examined a set of boron doped Cz samples from a standard ingot. The wafer surfaces are not passivated. Our results show that the difference between trap density in the passivated defect state minus trap density in the activated defect state is positively correlated to the interstitial oxygen concentration and in contradiction to⁸ positive for high oxygen concentration. The difference in the trap density plotted against the interstitial oxygen concentration is depicted in fig. 8. The examined wafers are standard boron doped and unpassivated Cz wafers. The interstitial oxygen concentration was determined by FT-IR. The defect was activated by an illumination of 1000 W/m^2 for 14 h and passivated by annealing the wafers at 300°C in the dark.

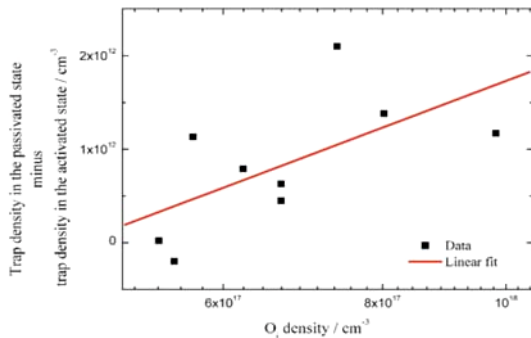


Figure 8: Trap density in passivated Cz-specific defect state minus trap density in activated defect state against interstitial oxygen concentration. Linear fit points out the positive correlation.

We observed a decrease of the trap density with the activation of the Cz-specific defect in seven of nine samples. This rules out an involvement of the activated state of the Cz-specific defect in the formation of trap centers. The positive correlation between the difference in the trap density and the interstitial oxygen concentration on the other hand is an indication, that oxygen plays an important role in trap centers, since oxygen is released from the BO_{2i} complexes by the heat treatment and the Cz-specific defect density is positively correlated to the oxygen concentration [18,19,20]. Thus the amount of oxygen which is released during the annealing should be positively correlated to the interstitial oxygen concentration, if boron is not the limiting component.

Since also boron is released by the annealing, boron could also contribute to the trap density. This is checked in fig. 9: The slightly negative trend of the difference against the boron concentration is leading to the conclusion that oxygen is the dominant factor. This

conclusion is supported by the fact that gallium doped Cz wafers show trap densities of the same magnitude as boron doped wafers [8].

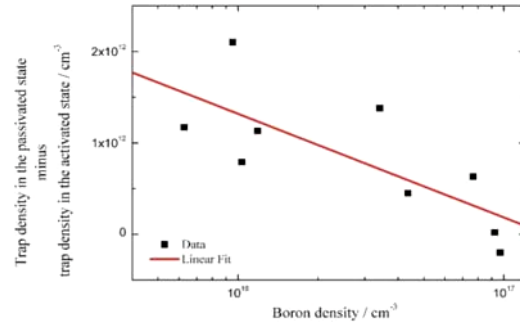


Figure 9: Trap density in passivated minus trap density in activated defect state against boron concentration. The linear fit illustrates that an increase of the difference with boron concentration can be excluded.

3.4 High temperature annealing and the trap density

The possible occurrence of thermal donors in Cz-silicon is a well known fact (see e.g. [21] for an overview). Thermal donors are formed during slow cooling between 300°C and 600°C and can be destroyed by an annealing step at 800°C , whereas so called ‘new thermal donors’ (see e.g. [20] for an overview) and oxygen precipitates are generated around 800°C . ‘New thermal donors’ differ from ‘old’ thermal donors in their ionization energy, the maximum generation temperature and the relation to carbon [21].

In [8] thermal donors were mentioned as a possible origin of trap centers. In order to scrutinize this hypothesis, the trap densities of $(250 \pm 5) \mu\text{m}$ thick as-cut Cz wafers from standard ingots with sufficiently high oxygen content were determined before and after an annealing step at 800°C . The total doping density before and after the annealing was measured by means of four point probe measurements. The doping density was increased by the annealing from $9.06 \times 10^{14} \text{ cm}^{-3}$ to a value close to the by the manufacturer specified doping density of $2.5 \times 10^{15} \text{ cm}^{-3}$. The increase of the doping concentration clearly indicates that thermal donors were destroyed during the annealing step. The injection dependent lifetime measurements before (blue) and after (red) the annealing are displayed in fig. 10.

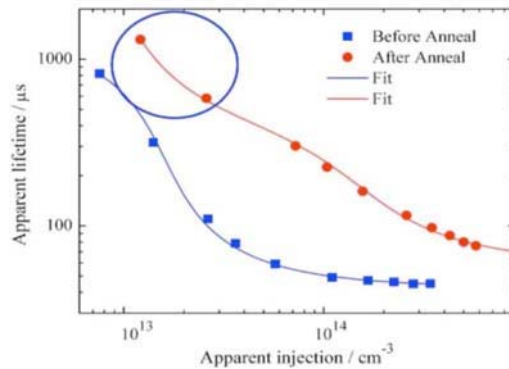


Figure 10: Injection dependent lifetime before (blue) and after (red) annealing. The dots and squares represent the experimental data.

Due to the increasing slope with decreasing injection between the two points with the lowest injection (see circle), an extended Hornbeck-Haynes model with two different trap centers [3] must be applied for a satisfactory fit. This characteristic was observed in a couple of Cz wafers, which were annealed at 800 °C. The trap density with the energy level of 0.58 eV remains with $1.63 (1,76) \times 10^{13} \text{ cm}^{-3}$ before (after) the anneal rather unchanged, whereas the trap density with the energy level of 0.72 eV is drastically increased by the anneal from $2.1 \times 10^{13} \text{ cm}^{-3}$ to $1.77 \times 10^{13} \text{ cm}^{-3}$.

Therefore oxygen precipitates and ‘new thermal donors’ arise as possible oxygen related origin of trap centers, because both can be generated around 800° C. This suggestion is also supported by the data in [22], which showed a positive correlation between doping density and trap density and the observation in [23], that an increased doping density in turn enhances the formation of precipitates.

3.4 Trap density and diffusion length in solar cells

In recent papers [24,4] a negative correlation between the trap density in as-cut wafers and the diffusion length in processed solar cells was reported for some examples. We studied the trap density across a multicrystalline ingot and found that the trap density itself and, in parallel, its correlation to the diffusion length is decreasing from the bottom to the top of the ingot.

The trap density measured on a vertically cut wafer from the bottom region of a directionally solidified multicrystalline ingot with a doping concentration of $5.5 \times 10^{15} \text{ cm}^{-3}$ is shown in fig. 11. In comparison, the image of the reciprocal lifetime of the solar cell processed on a neighboring wafer was calculated from an SR-LBIC [25] measurement and is depicted in fig. 12.

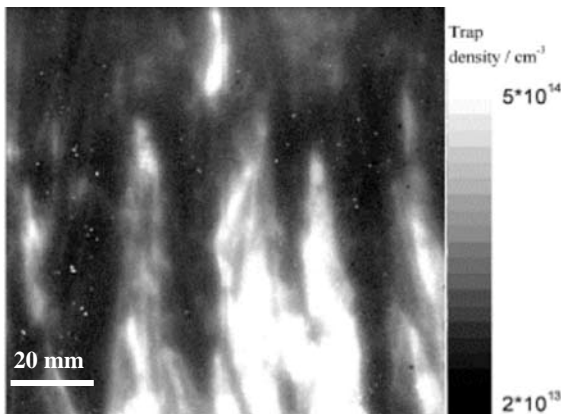


Figure 11: Trap density image of a vertically cut as-cut wafer from the bottom region of a multicrystalline standard ingot. The bottom of the ingot is at the bottom of the image.

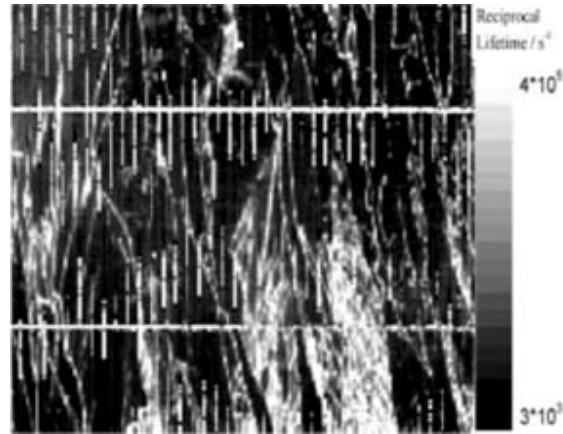


Figure 12: Image of the reciprocal lifetime of the solar cell, which was processed from the wafer in fig. 11. The reciprocal lifetime was calculated from SR-LBIC measurements.

The decrease of average trap density with height and the spatial correlation between trap density and diffusion length in this wafer are presented in fig. 13 and fig. 14.

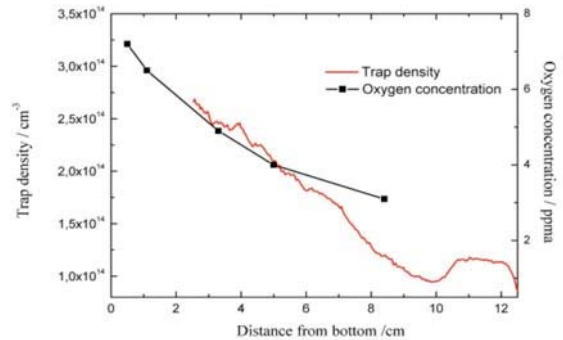


Figure 13: Trap and interstitial oxygen density against height. The trap density is decreasing with increasing distance from the bottom except for the topmost region.

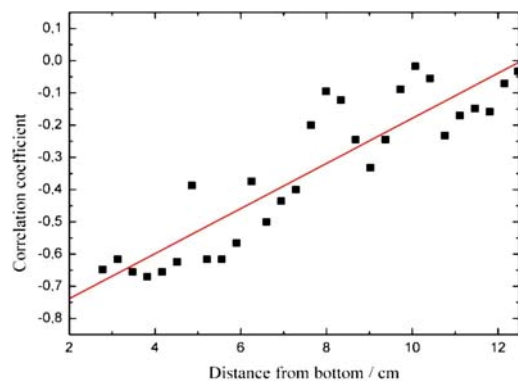


Figure 14: Correlation coefficient between trap density in the as-cut wafer and diffusion length in the processed solar cell. The correlation is quite high in the bottom region and decreases with height.

Results showing the same trends were measured by CDI/ILM on other ingots. Interestingly, measurements done by QSSPC in the literature [26] show different height dependent trap density profiles. This may be caused by differing impurity profiles in the respective crystals investigated or by the different measurement conditions: QSSPC measures under quasi steady state

conditions whereas CDI/ILM measures under steady state conditions, trapping effects could thus be seen differently if traps are emptied slowly compared to typical minority carrier lifetimes.

Oxygen is the only known major impurity in silicon with a segregation coefficient greater than 1 [20]. Therefore its concentration decreases from the bottom to the top of a multicrystalline block, which crystallizes from the bottom to the top. This behaviour was confirmed by FT-IR measurements of the interstitial oxygen concentration $[O_i]$ on a wafer parallel to the investigated one in the figures 10 – 13: $[O_i]$ decreases from 6 ppm in 1 cm distance from the bottom to 3.5 ppm in 6 cm distance from the bottom falling to values below the detection limit at greater height (see fig. 13). Since oxygen correlated defects are limiting the diffusion length in the bottom region [27] whereas various impurities are dominating in the top region [28], the decrease of the trap density and its correlation to the diffusion length with height supports the notion that the traps in multicrystalline as in Czochralski silicon [8] are strongly correlated to oxygen related defects.

4 CONCLUSIONS

We showed that structural crystal defects are necessary but not sufficient for the existence of high trap densities in some multicrystalline silicon samples. This could be due to the fact that structural crystal defects act as precipitation sites for impurities and traps mark in particular decorated defects. Metallic impurities were demonstrated not to increase, rather decrease the trap density, and thus can be ruled out as single origin of traps. Also the Cz-specific defect and thermal donors were shown not to be the main origin of trap centers. The comparison of the trap density in the activated Cz-specific defect state and the passivated state gave an indication that oxygen plays an important role in the formation of trap centers in Cz-silicon. The increased trap density in Cz-silicon after an 800 °C annealing gave rise to the suggestion that oxygen precipitates or clusters such as the ‘new thermal donors’, which can be generated at 800 °C, act as traps. The hypothesis, that oxygen is at least partly responsible for the existence of traps, was also supported by the height dependence in multicrystalline silicon ingots of the correlation between trap density in as-cut wafers and diffusion length in solar cells. Thus, the origin of increased trap densities in multicrystalline silicon could be structural crystal defects, which are highly decorated with oxygen precipitates or clusters and trap density measurements could be a well suited technique to detect these defects.

5 ACKNOWLEDGEMENT

We would like to thank Holger Habenicht and Daniel Schwaderer for fruitful discussions, Tobias Kalden, Daniel Kray, Mirosława Kwiatkowska, Harald Lautenschlager and Antonio Leimenstoll for sample preparation and Tonio Buonassisi for providing samples. We also thank the “CrystalClear” project funded by the European Commission under Contract No. SES6-CT_2003-502583 and especially Gianluca Coletti for providing some of the samples and the data on oxygen

concentrations in the vertically cut wafers. These investigations were partly funded by the German Ministry for Research and Education under Contract No. 01SF0401.

REFERENCES

- [1] D. Macdonald and A. Cuevas, Applied Physics Letters **74**, 1710-2 (1999).
- [2] D. Macdonald and A. Cuevas, Solar Energy Materials and Solar Cells **65**, 509-16 (2001).
- [3] P. Pohl, J. Schmidt, C. Schmiga, and R. Brendel, Journal of Applied Physics **101**, 1-11 (2007).
- [4] P. Gundel, M. C. Schubert, and W. Warta, Proceedings of the 22nd EU-PVSEC, Milan, Italy, 2007, p. 1608-12.
- [5] H. Y. Fan, Physical Review **92**, 1424-8 (1953).
- [6] J. R. Haynes and J. A. Hornbeck, Physical Review **100**, 606-15 (1955).
- [7] M. C. Schubert, S. Riepe, S. Bermejo, and W. Warta, Journal of Applied Physics **99**, 114908/1-6 (2006).
- [8] J. Schmidt, K. Bothe, and R. Hezel, Applied Physics Letters **80**, 4395-7 (2002).
- [9] P. Pohl, J. Schmidt, K. Bothe, and R. Brendel, Applied Physics Letters **87**, 142104-1-3 (2005).
- [10] M. C. Schubert, S. Riepe, and W. Warta, Proceedings of the 21st EU-PVSEC, Dresden, Germany, 2006, p. 629-33.
- [11] M. C. Schubert, S. Pingel, M. The, and W. Warta, Journal of Applied Physics **101**, 124907/1-5 (2007).
- [12] T. F. Cizek and T. H. Wang, Journal of Crystal Growth **237-239**, 1685-91 (2002).
- [13] G. Coletti, L. J. Geerligs, and P. Manshanden, Proceedings of the 22nd EU-PVSEC, Milan, Italy, 2007, p. 989-993.
- [14] D. H. Macdonald, Dissertation Thesis, The Australian National University, 2001.
- [15] H. Fischer and W. Pschunder, Proc. Idh. Eff. PVSC, Palo Alto, CA, 1973, p. 404-11.
- [16] J. Knobloch, S. W. Glunz, V. Henninger, W. Warta, W. Wetzling, F. Schomann, W. Schmidt, A. Endrös, and K. A. Münzer, Proceedings of the 13th EU-PVSEC, Nice, France, 1995, p. 9-12.
- [17] J. Schmidt, K. Bothe, and R. Hezel, Proceedings of the 29th IEEE-PVSC, New Orleans, Louisiana, USA, 2002, p. 178-81.
- [18] S. W. Glunz, S. Rein, W. Warta, J. Knobloch, and W. Wetzling, Proceedings of the 2nd WC PVSEC, Vienna, Austria, 1998, p. 1343-6.
- [19] J. Schmidt, A. G. Aberle, and R. Hezel, Proceedings of the 26th IEEE-PVSC, Anaheim, California, USA, 1997, p. 13-18.
- [20] T. Yoshida and Y. Kitagawara, Proceedings of the 4th International Symposium on High Purity Silicon, San Antonio, Texas, USA, 1996, p. 450-4.
- [21] A. Borghesi, B. Pivac, A. Sassella, and A. Stella, Journal of Applied Physics **77**, 4169-244 (1995).
- [22] D. Macdonald, M. Kerr, and A. Cuevas, Applied Physics Letters **75**, 1571-3 (1999).
- [23] S. Matsumoto, I. Ishihara, H. Kaneko, H. Harada, and T. Abe, Appl. Phys. Lett. **46**, 957 (1985).

- [24] M. C. Schubert and W. Warta, Progress in Photovoltaics: Research and Applications **15**, 331-6 (2007).
- [25] W. Warta, J. Sutter, B. F. Wagner, and R. Schindler, Proceedings of the 2nd WC PVSEC, Vienna, Austria, 1998, p. 1650-3.
- [26] R. A. Sinton, T. Mankad, S. Bowden *et al.*, Proceedings of the 19th EU-PVSEC, Paris, France, 2004.
- [27] D. Karg, Thesis Thesis, Universität Erlangen-Nürnberg, 1999.
- [28] T. Buonassisi, A. A. Istratov, M. D. Pickett, M. Heuer, J. P. Kalejs, G. Hahn, M. A. Marcus, B. Lai, Z. Cai, S. M. Heald, T. F. Ciszek, R. F. Clark, D. W. Cunningham, A. M. G. R. Jonczyk, S. Narayanan, E. Saunar, and E. R. Weber, Progress in Photovoltaics **14**, 513-531 (2006).